A global survey of cloud overlap based on CALIPSO and CloudSat measurements

Jiming Li,[1] Jianping Huang,[1,*] Knut Stamnes,[2]
Tianhe Wang,[1] Qiaoyi Lv[1], Hongchun Jin[1]

[1]Key Laboratory for Semi-Arid Climate Change of the Ministry of Education, College of Atmospheric Sciences, Lanzhou University, Lanzhou, China

[2]Department of Physics and Engineering Physics, Stevens Institute of Technology, Hoboken, NJ, USA

Running Head: Statistical properties of cloud overlap

*Corresponding author: Jianping Huang, Key Laboratory for Semi-Arid Climate Change of the Ministry of Education, College of Atmospheric Sciences, Lanzhou University, Lanzhou, Gansu 730000, China. (hjp@lzu.edu.cn)

Abstract

Based on four year' 2B-CLDCLASS-Lidar (Radar-Lidar) cloud classification and 2B-FLXHR-LIDAR radiative products from CloudSat, this study evaluate the co-occurrence frequencies of different cloud types, analyzes their along-track horizontal scales and radiative effects, moreover, utilize the vertical distributions of cloud type to preliminary evaluate the cloud overlap assumptions.

The statistical results show that high cloud, altostratus, altocumulus and cumulus are much more likely to co-exist with other cloud types. However, stratus (or stratocumulus), nimbostratus and convective clouds are much more likely to exhibit individual features. For global averages, Altostratus-over-Stratus/Stratocumulus cloud system has maximum horizontal scale (17.4 km) and standard deviation of scale (23.5 km), while Altocumulus-over-Cumulus has minimum scale (2.8 km) and standard deviation (3.1 km). By considering the weight of each multilayered cloud type, we find that the global mean cloud radiative effects of multilayered cloud systems during daytime are about -41.3 W/m^2 and -50.2 W/m^2 at TOA and surface (contribution: about 40%), respectively. Radiative contributions of High-over-Altocumulus and High-over-Stratus/Stratocumulus (or Cumulus) to whole multilayered cloud systems are dominant due to their more frequent occurrences.

After considering the overlap of cloud types, the cloud fraction based on the random overlap assumption is underestimated over the vast ocean except in the west-central Pacific Ocean warm pool. Obvious overestimations are mainly occurring over land areas in the tropics and subtropics. The investigation therefore indicates that incorporate overlap information of cloud types based on Radar-Lidar cloud classification into the overlap assumption schemes used in the current GCMs possible be able to provide an better predictions for total cloud fraction.

1. Introduction

As the most important regulators of the Earth's climate system, clouds may significantly affect the radiation budget, the hydrological cycle and the large-scale circulation of the Earth (Hartmann et al., 1992; Stephens, 2005). However, due to an incomplete knowledge of the underlying physical processes, clouds are still poorly represented in climate and weather models (Zhang et al., 2005), and thus are considered as the major source of uncertainty in predictions of climate change by general circulation models (GCMs) (Cess et al., 1990).

Cloud type, which is of the important cloud macro-physical properties, is of particular significance for the earth's radiation budget and hydrological cycle. Different cloud types are governed by different kinds of atmospheric motions and have different microphysical properties, thus can result in markedly distinct cloud radiative effects (Ackerman et al., 1988; Betts and Boers, 1990; Hartmann et al., 1992) and precipitation forms (or intensities). However, multilayered cloud systems, with two or more cloud types occurring simultaneously over the same location but at different levels in the atmosphere have been frequently reported by surface and aircraft observations (Tian and Curry, 1989). The frequent co-occurrences of different cloud types in the atmosphere intensify the complexity of present cloud climatology studies. For example, the effects of individual cloud type on the surface and atmospheric radiation budgets depend on whether other clouds are also present above or below them. In addition, cloud overlap variations also can significantly change atmospheric radiative heating/cooling rates, atmospheric temperature, hydrological processes, and daily variability (Chen and Cotton, 1987; Morcrette and Jakob, 2000; Liang and Wu, 2005). Therefore, to further improve radiation calculations of climate prediction models and help understand cloud physical processes and evaluate the schemes for generating clouds in those models, it is necessary to know the amount and distribution of each cloud type, especially a detailed description of the co-occurrence of different cloud types and their statistical properties.

Until now, many related works with cloud type and cloud overlap, which based on several fundamentally different types of passive observational datasets (typically the International Satellite Cloud Climatology Project (ISCCP) and surface observer reports), have focused on the geographic distributions and long-term variations of different cloud types (e.g. Rossow and Schiffer, 1991; Rossow and Schiffer,1999; Hahn et al., 2001; Warren et al., 2007; Eastman et al., 2011; Eastman et al., 2013), and their radiative effect investigations (Hartmann et al., 1992; Chen et al., 2000; Yu et al., 2004), or specially aimed at the cloud properties retrieval of multilayered cloud by using multi-channel measurements from passive sensors (Chang and Li, 2005a, Chang and Li, 2005b; Huang et al., 2005; Huang et al., 2006a; Huang et al., 2006b; Minnis et al., 2007), and the statistics of cloud overlap based on the surface weather reports and the measurements from the ground-based cloud radar (Warren et al., 1985; Hogan and Illingworth, 2000; Minnis et al., 2005). However, these studies have non-negligible limitations and uncertainties due to passive detection methods and cloud classification algorithms generally fail to effectively detect multilayered clouds. First, the existence of overlapping cloud layers may cause the upper clouds to be hidden from the view of a ground weather reporter, and lower clouds to be hidden from the view of a passive satellite which leads to a significant underestimation of high and low cloud frequencies by surface observer reports and ISCCP, thus introduce significant biases in the trends analysis of cloud-type cover, retrievals of cloud properties and evaluation of cloud radiative effects of different cloud types. Second, most of these studies are limited to specific locations and time periods or multilayered cloud systems, systematic researches about the co-occurrence statistics of different cloud types on a global scale still have received much less attention.

Fortunately, the launch of the millimeter wavelength cloud profiling radar (CPR) on CloudSat (Stephens et al., 2002) and the cloud-aerosol lidar with orthogonal polarization (CALIOP) (Winker et al., 2007) on CALIPSO in late April 2006 provide us an unprecedented opportunity for detailed studying the three-dimensional structures of cloud on a global scale. Since becoming available in the middle of June 2006, CALIPSO and CloudSat data have been widely used to investigate the three-dimensional distributions and structures of hydrometeor, and improve the cloud overlap assumption used in GCMs (e.g. Barker, 2008; Luo et al., 2009; Kato et al., 2010; Li et al., 2011). By using Radar-only cloud classification product (that is, 2B-CLDCLASS dataset from CloudSat), Sassen and Wang (2008) already have depicted the geographical distributions of each cloud type and provided their global average occurrence frequency. In this study, we will pay more attention to investigate the co-occurrence frequencies of different cloud types, analyze their along-track horizontal scales and radiative effects by using the latest cloud classification and radiative fluxes products based on the combined measurements of these two active sensors. At last, we also will preliminary evaluate how well the cloud overlap assumptions can characterize the overlap of two apparently separated cloud types. Although some statistical results are in reasonable agreement with previous works, additional new insights are also gained in this investigation. It is hoped that these new results will be useful for future GCM evaluation and improvement.

The study is organized as follows. The dataset used is described in Section 2. Section 3 gives the zonal distributions and global statistics of co-occurrence frequency of different cloud types, then discusses their along-track horizontal scales and radiative effects. The evaluation the performance of cloud overlap assumptions based on co-occurrence frequency of cloud types is presented in the section 4.

2. Data

In the following study, four years (2007-2010) of data from the latest release of the CloudSat 2B-CLDCLASS-Lidar (version 1.0) product, which is referred as Radar-Lidar cloud classification, and 2B-FLXHR-LIDAR product are collected to analyze cloud types and discuss their co-occurrence frequency, horizontal scales and radiative effects.

It is well known that the ISCCP uses a combination of cloud top pressure and cloud optical depth to classify clouds into cumulus stratocumulus, stratus, altocumulus, altostratus, nimbostratus, cirrus/cirrostratus, and deep convective clouds. However, the traditional surface observations identify cloud by using some basic features (e.g. base height, horizontal and vertical dimensions, precipitation types) of the major cloud types (World Meteorological Organization, 1956; Parker, 1988; Moran et al., 1997). Based on these basic cloud characteristics, Wang and Sassen (2001) classified cloud types into eight classes by combining the ranging capabilities of active sensors (Radar and Lidar) and the auxiliary measurements from the other passive sensors (such as, infrared and microwave radiometers), and further indicated the overall agreement (about 70%) between the results from their algorithm and surface visual observations from the Southern Great Plains (SGP) CART site.

Based on the algorithm presented by Wang and Sassen (2001), the Radar-Lidar cloud classification identifies the cloud types by using two main steps. First, combined radar and lidar cloud mask results are used to find a cloud cluster according to their persistence in the horizontal and vertical directions. By performing the cloud clustering analysis, a CloudSat granule may be divided into a number of cloud clusters depending on the cloud systems present. Once a cloud cluster is found, cloud height and phase, maximum effective radar reflectivity factor (Ze) and its temperature, as well as the occurrence of precipitation, are then determined. Second, the cluster mean properties as well as spatial inhomogeneties in terms of cloud top height, lidar and radar maximum signals are sent to a fuzzy classifier to classify the cluster into one cloud type with an assigned confidence level. To improve classification flexibility, a combination of rule based and fuzzy logical based classification is used in this algorithm. The cloud phase determination is based on rule-based logics and the cloud type classification is mainly based on the fuzzy logics (See Wang et al., Level 2 combined radar and lidar cloud scenario classification product process description and interface control document, version 1.0, 2013, available at http://www.cloudsat.cira.colostate.edu/dataICDlist.php?go=list&path=/2B-CLDCLSS-LIDAR). The cloud types provided by this product (version 1.0) include: high cloud (High), altostratus (As), altocumulus (Ac), stratus (St), stratocumulus (Sc), cumulus (Cu), nimbostratus (Ns) and deep convective (Dc) clouds. The High cloud type includes cirrus, cirrocumulus and cirrostratus, and the Cu cloud type represents cumulus congestus and fair weather cumulus. Followed the study of Sassen and Wang (2008), we also combine two level cloud types (St and Sc) as St+Sc in present study in order to compare the results with other datasets. Due to combine the unique complementary capabilities of Cloud profile radar (CPR) from CloudSat and space-based polarization lidar (CALIOP), some CPR weaknesses (e.g. high surface contamination in the lowest three to four vertical bins of CPR, and lower sensitivity to optically thin clouds) will be minimized in the latest Radar-Lidar cloud classification product, this eventually led to the significant improvement for High (cirrus or cirrostratus) and lower cloud types (such as, St, Sc and Cu) identification in the 2B-CLDCLASS-Lidar product (please see Table 5).

By using CloudSat microphysical retrievals, combined CloudSat/CALIPSO cloud mask and also utilizes lidar-based aerosol retrievals as inputs to a broadband, two-stream, plane-parallel, adding and doubling radiative transfer model, the 2B-FLXHR-LIDAR product provide us the calculated radiative fluxes and atmospheric heating rates at 240 m vertical increments (Henderson et al., 2013). Incorporate the radiative influence of optically thin and low clouds that went undetected by CloudSat significantly improved agreement between 2B-FLXHR-LIDAR calculations and CERES observations. Henderson et al. (2013) showed that global mean outgoing shortwave radiation (OSR) and outgoing longwave radiation (OLR) estimated from collocated CERES observations and 2B-FLXHR-LIDAR calculations agree to within 4 and 5W/m^2, respectively, with root-mean-square differences of 6W/m^2 and 16W/m^2 on monthly/5° scales. Due to the passive sensors largely fail to resolve the cloud vertical overlap, thus the 2B-FLXHR-LIDAR product derived from these two active sensors is considered as a vital dataset to examine radiative heating features in the atmosphere, and study the variations of flux and heating rate caused by cloud vertical overlap (L'Ecuyer et al., 2008; Haynes et al., 2013). In this investigation, we only focus on the radiative effects of different multilayered cloud types at the top of atmosphere (TOA) and surface during daytime by using this dataset.

Following cloud parameters in the 2B-CLDCLASS-Lidar product are used in this study: Cloud layer (CL), Cloud Layer Type (CLTY). In 2B-FLXHR-LIDAR product, only the TOACRE (cloud radiative effect at TOA) and BOACRE (cloud radiative effect at surface) are used. In order to map the regional variability of the studied variable, we group the global area into 2°×2° grid boxes in order to collect a sufficient number of samples in each grid box. Following the definitions of cloud fraction and cloud amount by Hagihara et al. (2010), the cloud-type fractions (amounts) in a given grid box are defined as the number of a certain cloud type profiles divided by the number of total cloud profiles (or total sample profiles) collected in this box. In this investigation, we only provide the annual average cloud properties of different cloud-types overlap in view of small seasonal variations. In addition, the comparisons of four years' average cloud fraction for different cloud types between day- and night-time also are provided in the tables of this investigation. It is worth noting that the full diurnal cycle cannot be captured by CALIPSO and CloudSat. Thus, the day-night comparisons of cloud fraction are referred as the comparison between the two overpass times of these satellites. In addition, Sassen et al. (2009) showed that the observed diurnal variations of cirrus by CALIPSO mostly reflect real cloud process even if the strong solar noise signature possible impacts the comparisons of cloud types between day and night in present study, especially for cirrus. For other cloud types, the uncertainty caused by the daylight noise for Lidar may be smaller. Thus, the calculated annual mean cloud fractions for different cloud types in this investigation still are reliable.

3. Simultaneous co-occurrence of different cloud types

3.1. Zonal distributions of cloud overlap

Multilayered cloud systems frequently occur in the atmosphere. Our statistical results show that the seasonal variations of multilayered cloud fractions are small, the seasonal globally averaged values range from 25% to 28%. These results are comparable with the multilayered cloud fractions (about 27%) from the Geoscience Laser Altimeter System (GLAS) (Wylie et al., 2007). Further, we plot the global and zonal distributions of annually averaged multilayered cloud fraction (see Fig. 1). In Fig. 1a, the high-value and low-value centers of multilayered cloud fractions are very obvious. For example, the equatorial central South America, western Africa, Indonesia and the west-central Pacific Ocean warm pool are typical high-value centers. For zonal distributions (Figure 1b), there are three obvious peaks in zonal mean patterns, one major peak in the tropics, two minor peaks in the middle latitudes, and two local minima in the subtropics. The local maximum during spring (black thicker line) in the northern mid-latitudes that may be a result of high-level dust transport being misidentified as high ice clouds or a manifestation of actual influences of dust on ice nucleation (Chen et al., 2010; Yu et al., 2012; Yuan and Oreopoulos, 2013).

In all multilayered clouds, we further pick out the annual most frequently multilayered cloud systems and provide their zonal distributions (Figure 2). It is worth noting that the overlap from the same cloud type (e.g. High+High) is not important for numerical climate simulation due to their similar cloud properties and temperatures when they are not separated too far. Thus, treating them as a single layer cloud may not introduce severe errors in the calculation of their cloud propertie (Wang and Dessler, 2006). Figure 2 clearly indicates that the zonal patterns of different combinations of different cloud types are very different. For example, multilayered cloud systems which include high clouds either have one peak in the tropics (High+Ac and High+Cu) or three peaks in the tropics and mid-latitudes (High+St/Sc, High+Ns and High+As). The high clouds in the major peak in the tropics may be caused by the large-scale ascent or by the dissipating deep convection. However, gentle large-scale ascent and ice cloud production from frontal convection are likely responsible for the two minor peaks of multilayered cloud systems in the mid-latitudes storm tracks. Besides these combinations of cloud types, As-over-strati-form clouds or Ac-over-strati-form clouds also tend to concentrate in the mid-latitudes (60 $^{\circ}$ and pole-ward). In fact, the distributional patterns of cloud in different geographical regimes may depend on environmental factors in these regimes, such as sea surface temperature, lower tropospheric stability, and vertical velocity (Klein and Hartmann, 1993; Norris and Leovy, 1994). In recent work, by studying the relations between various cloud types and sea surface temperature over the tropical oceans, Behrangi et al. (2012) indicated that as SST increases, the fraction of multilayered clouds increases up to an SST of 303 K, and then decreases for SSTs greater than 303 K. The ranges of SST are very different for different combinations of cloud types, such as, high cloud over strati-form or nimbostratus tend to occur between 292 and 294 K, but high cloud over altocumulus or altostratus or cumulus tend to exist between 302 and 304 K even though almost all of them have major peak values in the tropics. In addition, Yuan and Oreopoulos (2013) further indicated that large-scale pressure vertical velocity is found to anti-correlate well with the percentage of multilayered cloud systems. Strong subsidence thus favors low cloud formation and suppresses ice cloud generation, explaining why multilayered clouds are very infrequent over major stratocumulus dominated oceanic areas around 30 º latitudes.

However, these multilayered cloud systems are very difficult to be effectively detected by passive satellites (such as, ISCCP) and surface weather reporters, especially during the nighttime and for those cloud systems which include very thin cirrus (Sassen and Cho, 1992; Liao et al., 1995). For example, when a high-level transparent cirrus cloud overlies a boundary layer stratus cloud, the retrieved cloud top heights typically lie between the cirrus and the stratus cloud heights (e.g., Baum and Wielicki, 1994) leading to mis-assignment of cloud types by ISCCP. For cloud properties retrieval, the influence of liquid water clouds and precipitation on the radiances observed at the top of the atmosphere (TOA) also is one of the greatest impediments to accurately determining cloud ice mass for multi-layered systems with ice clouds above water clouds (Huang et al., 2006a).

3.2. Global statistics of cloud overlap

Global average overlapping percentages of different combinations of cloud types over land and ocean during daytime and nighttime are provided in Tables 1 and 2, respectively. These tables show that high cloud, As, Ac and cumulus types are much more likely to co-exist with other cloud types regardless of day or night, land or ocean. The frequency of High-over-Ac even may exceed the frequency of single-layered altocumulus cloud, indicating that these two types actually exhibit a stronger meteorological association. However, due to under large-scale subsidence regions, stratus/stratocumulus and nimbostratus are much more likely to exhibit individualism features, particularly for stratus/stratocumulus over the ocean. For convective clouds, they are also typically single. Although cumulus occurs in unstable air whereas altostratus occurs in stable air, there is still a small percentage of overlap between them. Globally, 44% (50%) and 35% (39%) of low clouds (St/Sc +Cu) over land and ocean during daytime (nighttime) are overlapped by other cloud types aloft, respectively. About 23% (26%) and 20% (25%) of low clouds over land and ocean during daytime (nighttime) are connected with high clouds, respectively. These percentages are comparable with those (about 30%) provided by Yuan and Oreopoulos (2013). In addition, it is worth noting that high clouds also include cirrostratus and cirrocumulus, thus the overlap fraction of deep convection lying below high clouds is about 29%, and larger than the fraction (about 24%) of cirrus-over-convection clouds based on ICESat/GLAS (Geoscience Laser Altimeter System) (Wang and Dessler, 2006).

Based on above figures and tables, we plot the global distributions of annual mean dominant cloud types and their cloud fractions (see Fig.3a-3b). Here, the cloud types include single-layered and multilayered cloud systems. The Figure 3c-3d shows that the global distributions of the annual mean dominant multiple cloud types and corresponding cloud amounts. It is evident from Fig.3a-3b that stratocumulus and stratus are the dominant cloud types worldwide, particularly over the ocean. High clouds are mainly concentrated in the tropics and subtropics. In addition, over Antarctica, the most frequent cloud type is altostratus. These results are in reasonable agreement with the findings based on the ISCCP D1 dataset (Doutriaux-Boucher and Seze, 1998). But, Fig.3a-3b also shows that altostratus also prevails over the arid/semi-arid land in the Northern Hemisphere, such as, the northwestern part of China and North America. In contrast, altocumulus is the dominant cloud type over the arid/semi-arid land of the Southern Hemisphere, such as Australia and the southern part of Africa. However, all these features are not observed by Doutriaux-Boucher and Seze (1998) using the ISCCP D1 dataset. In fact, the obvious regional and seasonal variations of altocumulus and altostratus possible are related with the frequency of dust activities (Choi et al., 2009). In addition, over some deserts (such as the Sahara Desert), the most prevalent cloud type is a low level cloud (stratocumulus and stratus) in ISCCP D1 rather than a high cloud in our results. This discrepancy may be due to inadequate identification of airborne dust as low level clouds by ISCCP, as suggested by the low values of effective droplet radius reported by Han et al. (1994) over these regions.

General speaking, the High-over-St/Sc and High-over-Cu cloud systems are more popular over the vast ocean of the tropics and mid-latitudes, while High-over-Ac cloud systems tend to exist over the land in the same latitudes (see Fig.3c). Especially, the As-over-Cu only occurs at the northwest of China. In addition, the As-over-St/Sc cloud systems are dominant in the high-latitudes. Figure 3d shows the multilayered cloud-type amount, defined as the ratio of the cloud fraction of one multilayered cloud combination to the cloud fraction of total multilayered cloud systems. In addition, we note that there is still some multilayered cloud systems (almost is High-over-St/Sc) over the major stratocumulus dominated oceanic areas, which are generally unfavorable to upper level cloud formation due to persistent strong subsidence. The major source of high cloud possible is topography-driven gravity wave activity, advection from neighboring tropical convection centers such as the Amazon Basin, the Congo Basin, or ascent associated with mid-latitude fronts.

3.3. Along-track horizontal scales and radiative effects of cloud overlap

The horizontal scale of a multilayered cloud system along the CALIPSO/CloudSat track is determined by calculating the number of continuous profiles (N), which include same combination of cloud types in the vertical column. Considering the 1.1 km along-track resolution of CPR measurements, the along-track scale (L in km) of a multilayered cloud system is $L = N \times 1.1$ (Zhang et al., 2014).

Figure.4a-4d presents the zonal variation of cloud along-track horizontal scales for these multilayered cloud systems and their probability distribution function (PDF). As described by the Figure 4a-4b, the High+St/Sc, As+St/Sc, High+Ns and High+Dc cloud systems have obvious zonal variations. Among them, High+St/Sc and As+St/Sc have minimum scales (about 10 km) at tropics and maximum scales (reach 20km) in the latitudes of 40° pole-ward (that is, storm track). However, the along-track horizontal scales of High+Ns and High+Dc decrease from tropics to polar region. For other cloud systems, the zonal variations of their scales are small, especially for High+Cu, As+Cu and Ac+Cu (around 3km). We also provide the global average along-track horizontal scales and standard deviation (STD) of these cloud systems in Figure 4c-4d. Generally speaking, As+St/Sc has maximum scale (17.4 km) and STD (23.5 km), while Ac+Cu has minimum scale (2.8 km) and STD (3.1 km). Based on the relative larger STDs than mean scales, it is clear that the along-track horizontal scales of these cloud systems all have larger variation range on a global extent. By assuming a typical grid resolution of 1° in global climate models, we find that all multilayered cloud types cannot be resolved by global climate models. Those multilayered cloud systems which include cumulus (such as, High+Cu, Ac+Cu and As+Cu) even cannot be captured by regional climate models with higher grid resolution (about 15 km).

Further, Figure 5a-5b shows that the zonal distributions of cloud radiative effect for these multilayered cloud systems at the top of atmosphere (TOA) during daytime. In addition, we also give the zonal distributions of weighted cloud radiative effect by taking into account the frequency of occurrence of each cloud type only during daytime (Figure 5c-5d). Although the zonal distributions of cloud radiative effect for these cloud systems are similar, that is, decrease from tropics to high-latitudes. However, their radiative effects can be grouped into several obvious different classes. For example, middle-over-low (such as, As+Sc/St and As+Cu) cloud systems have comparable radiative effect (maximum value: around -300 W/m^2), while high-over-low (such as, High+Sc/St and High+Cu) cloud systems have smaller radiative effect (maximum value: around -150 W/m^2). By considering the weight of each multilayered cloud type, we find that their contributions to cloud radiative effect of whole multilayered cloud system are different (Figure 5c-5d). At tropics, High+Ac and High+Cu contribute the cloud radiative effects for -9 W/m^2 and -8 W/m^2, respectively. Other types have obvious zonal distributions, their contributions range from 0 to -6 W/m^2. At mid-high latitudes, the some mid-over-low (such as, As+Sc/St) cloud systems are more important to regional energy balance, especially over the

Southern ocean regions. Similar with Figure 5, the Figure 6 presents the results at the surface during daytime. In summary, the trends are similar, but all cloud types have larger radiative effects at the surface than at TOA, that is, their effect would be an obvious surface cooling. It is clear that the energy differences of cloud radiative effects between surface and TOA stay in atmosphere and can significantly change atmospheric radiative heating/cooling rates and atmospheric temperature, but the impacts are very different for different multilayered cloud types. In atmosphere (Figure not shown), these cloud types all cause a weak atmospheric heating at low and middle latitudes (about 0.5-3 W/m^2 radiative changes), whereas weaker atmospheric cooling also can be seen at high-latitudes for some multilayered cloud types (e.g. As+Sc/St, Ac+Sc/St and High+Sc/St).

On a global scale, the ranges of their global mean radiative effect almost are between -100 W/m^2 to -350 W/m^2 except for High+Dc (black dots are mean values and lines present standard deviation in Figure 7a-7b). In the Figure 7c and 7d, the black bars present the weighted radiative effects of each cloud type at TOA and surface, respectively. Generally speaking, the global mean cloud radiative effects are about -103.1 W/m^2 and -118.8 W/m^2 at TOA and surface, respectively. The percentages of radiative contribution from multilayered cloud systems reach 40.1% (about -41.3 W/m^2) and 42.3% ((about -50.2 W/m^2) at TOA and surface, respectively. It is clear that the existences of multilayered cloud system are distinctly important to Earth's radiative energy balance. Further analysis show that two-layered and three-layered (or more layers) cloud systems contribute the total cloud radiative effect about -27.2 (-33.1 W/m^2) and -14.1 (-17.1 W/m^2) at TOA (surface), respectively. However, the radiative effects of ten multilayered cloud types which we study reach -22.7 W/m^2 and -27.1 W/m^2 at TOA and surface (contribution: 22%). The High+Ac and High+Sc/St (or Cu) have relative smaller effects than High+Dc and Ac+Sc/St (or Cu), but their contributions to the cloud radiative effect of whole multilayered cloud system still are maximum due to their more frequent occurrence or larger weights (see gray line in Figure 7c-7d), especially their widely distributions from tropics to middle latitudes (Figure 3). However, the other cloud types possible are important to the regional cloud radiative effects. For example, the mid-to-upper level cloud frequently coexists with boundary layer cloud (e.g. As+St/Sc and High+St/Sc) over the Southern ocean cause the overestimations of middle cloudiness by ISCCP, and are partially responsible for TOA shortwave radiation bias in the climate models over this region (Haynes et al., 2011).

4. Evaluation of cloud overlap assumptions based on cloud types

Based on the advantages of two active sensors, we also preliminary evaluate how well the cloud overlap assumptions can characterize the overlap of two apparently separated cloud types by using 2B-CLDCLASS-Lidar cloud type product. As we know, the cloud overlap assumption has been widely used to describe the real cloud vertical distribution and parameterization of the total cloud fraction in a given model grid box. Several basic cloud overlap assumptions have been proposed, such as, maximum, random, random-maximum and minimum overlap (Hogan and Illingworth, 2000). The most common cloud overlap scheme in current GCMs is called "random-maximum" overlap. It assumes that cloud layers separated by any clear layers are randomly overlapped while vertically-continuous cloud layers overlap maximally (Stephens et al., 2004). If given the cloud fractions of upper and lower layers as C_1 and C_2, the total cloud fractions of the two cloud layers based on these overlap assumptions thus are given by:

$$C_{random}=C_1+C_2-C_1\times C_2\ ,$$

$$C_{max}=\max\ (C_1,\ C_2),\ \text{and}$$

$$C_{min}=\min\ (1,\ C_1+C_2). \qquad (1)$$

In addition, if we know the real overlap fraction $C_{overlap}$, then the observed total cloud fraction C_{real} can be written as:

$$C_{real}=C_1+C_2-C_{overlap} \qquad (2)$$

However, Hogan and Illingworth (2000) proposed a simpler and more useful expression for the degree of cloud layer overlap (that is, exponential random overlap). In the expression, the mean observed cloud fraction of two cloud layers can be determined by the linear combination of maximum and random overlap in terms of an "overlap parameter" *a* as:

$$C_{real}=a\times C_{max}+(1-a)\times C_{random} \quad (3)$$

Here, the overlap parameter a is considered as a function of layer separation. If a=0 corresponds to random overlap and a=1 to maximum overlap. As C_{real} departs more and more from C_{max} (trends toward C_{min}), a becomes negative. But, in the case of vertically non-continuous cloud, they indicated that random overlap assumption works well. Based on the several months' data from ICESat/GLAS observations, Wang and Dessler (2006) showed that overlap difference between observed and based on random overlap still exist when describe the real overlap of two separated cloud types (vertical separation >0.5 km). However, their work only focused on the tropical area and is limited to simple cloud classification based on space-based lidar. To expand their study to the global extent and more complete cloud classification, we follow the study of Wang and Dessler (2006) to further estimate the overlap of two separated cloud types of each combination of different cloud types in each grid box, moreover evaluate the performances of random overlap assumption and calculate the overlap parameter a for each multilayered cloud type in each grid box.

In order to do this, we first group each multilayered cloud system. For example, for the High+St/Sc multilayered cloud systems in same grid box, we don't group them into many layers according to the vertical separation of two types for convenience, but only consider two layers and group all high clouds into the upper layer and all strati-from clouds are grouped into the lower layer. Then, four possible values for the combined cloud fraction of the two cloud types at different layers are calculated by assuming random overlap, maximum overlap, minimum overlap and actually observed. In view of random cloud overlap is extensively thought to better characterize cloud overlap behavior than minimum overlap and maximum overlap, here we only provide the difference of cloud fraction between random overlap and actually observed. At last, the overlap parameter a for each multilayered cloud types in each grid will be calculated based on the equation (3). However, it is worth noting that due to we don't group multilayered cloud types into many layers according to the vertical separation of two types, thus only one value of overlap parameter a for each multilayered cloud system in each grid is obtained. The a may be considered as the mean value of all overlap parameters at different layer separation. Here, we define the relative difference (RD) between random and real overlap for one of the multilayered cloud types as:

$$RD=(C_{random}-C_{real})/\,C_{real} \qquad (4)$$

In addition, the cumulative relative difference (CRD) between random and real overlap for all multilayered cloud types (about 17 different combinations of different cloud types) in each 2°×2° grid box is given by:

$$CRD=\sum_{i=1}^{17} RD^{i}\times w^{i} \qquad i=1, 2, 3 \ldots, 17 \qquad (5)$$

Similar with the definition of CRD, we define cumulative overlap parameter (COP) in each 2°×2° grid box as:

$$COP=\sum_{i=1}^{17} a^{i}\times w^{i} \qquad i=1, 2, 3 \ldots, 17 \qquad (6)$$

where w is the weight coefficient for one of multilayered cloud types in each 2°×2° grid box. It can be written as follows:

$$w^{i}=f^{i}/\sum_{i=1}^{17} f^{i} \qquad i=1, 2, 3 \ldots, 17 \qquad (7)$$

where f is the cloud fraction of each multilayered cloud type in every grid box.

Fig. 8a-8b show the zonal distributions of the relative difference for ten of the main multilayered cloud types and the cumulative relative difference of all multilayered cloud types (gray line). The results show that differences still exist even if random cloud overlap assumption is thought to better describe cloud overlap behavior than other schemes when the cloud layers appear to be separated. The cloud fractions based on the random overlap assumption are underestimated for High+St/Sc, As+St/Sc and Ac+St/Sc at all latitudes. These differences even exceed -5%. The cloud fraction of high-over-altocumulus system is overestimated at all latitudes. The peak values of difference are mainly located at mid- and high- latitudes in both Hemispheres and can reach 5%. For other types, the relative differences are smaller than for the above four types, and alternate with latitudes. In summary, the cumulative relative difference of all multilayered cloud types is small (gray lines), and almost is negative at the all latitudes. In the Figure 8c-8d, we further show the zonal distributions of overlap parameter for ten of the main multilayered cloud types and the cumulative overlap parameter of all multilayered cloud types. It is clear that the overlap parameters for High+St/Sc, As+St/Sc and Ac+St/Sc at all latitudes all are negative, indicate that their C_{real} depart from C_{max} (trend toward C_{min}) and a tendency for an even lower degree of overlap than that predicted by the random overlap assumption. Thus, the linear combination of maximum and random overlap assumptions, which has an exponential parameterization of overlap parameter a, possible are problematic due to negative overlap parameters at those regions, where above three multilayered cloud types are dominant, especially over the major stratocumulus dominated oceanic areas where the High+St/Sc accounts for 80% of multilayered cloud. However, the overlap parameters almost are positive for High+Ns and High+Ac. This indicates that their C_{real} more trend to take values anywhere between the C_{max} and C_{random}, thus the exponential random overlap can predict the real overlap of these two types very well. In summary, the cumulative overlap parameters of all multilayered cloud types (gray lines) almost are negative at the all latitudes. But, there are three points still need to be further interpreted. First, the cumulative overlap parameters at tropics and Nouthern Hemisphere have small values (even have positive values), thus random overlap or exponential random overlap still can works well. Second, at the Southern Hemisphere, the cumulative overlap parameters become larger and more trend toward C_{min}, thus it is difficult to provide better prediction by using the random overlap or exponential random overlap. This possible partially interpret why the climate model errors in TOA fluxes over the Southern Ocean are among the largest anywhere in the world (Trenberth and Fasullo, 2010). Third, the cloud overlap parameters are very different each other even if they possible belong to the similar cloud overlap systems (e.g. middle-over-low). For example, the overlap parameters of As+St/Sc and Ac+St/Sc over the Southern ocean are obvious distinct with As+Cu and Ac+Cu. Based on these results, we suggest that a linear combination of minimum and random overlap assumptions possible may further improve the predictions of real cloud fraction for those multilayered cloud types at the Southern Hemisphere (e.g. As+St/Sc and Ac+St/Sc), especially over the ocean of 40°S pole-ward. These results also further indicate that incorporating co-occurrence information of different cloud types on a global scale by using Radar-Lidar cloud classification into the overlap assumption schemes used in the current GCMs possible be able to provide an better predictions for vertically projected total cloud fraction. However, to apply cloud type information to test model output, we have to take into account that the cloud type definitions of the particular dataset which include a number of classification rules and assumptions. Thus, some further studies still are needed.

The global distributions and statistical results of the cumulative relative difference and the cumulative overlap parameter for all multilayered cloud types are shown in Fig. 9 and Table 3 and 4, respectively. The Figure 9a is for the cumulative relative difference, whereas the Figure 9b is for the cumulative overlap parameter. In Figure 9a, we find that the cloud fractions based on random overlap assumption main are underestimated over the vast ocean except the west-central Pacific Ocean warm pool. Obvious overestimations are mainly located at the lands of tropics and subtropics, particularly at the regions with low multilayered cloud fraction, such as equatorial central South America, southern and northern Africa, Australia and the Antarctic continent, where the high-over-altocumulus system is the dominant multilayered cloud type. This pattern indicates that land surface effects may favor an exponential random overlap (ERO). In Figure 9b, the distributions of the cumulative overlap parameter are similar with those results of cumulative relative difference. Negative overlap parameters also main occur over the vast ocean except the west-central Pacific Ocean warm pool. The typical negative high-values centers are correspondence with the major stratocumulus dominated oceanic areas very well. The positive overlap parameters almost locate the lands of tropics and subtropics and the Antarctic continent. Globally, by using the random overlap, the overlap fractions are overestimated by 24%, 21.9%, 30% and 133.3% for high clouds over altostratus, strati-form clouds, nimbostratus, and or altocumulus over strati-form clouds over land during daytime, respectively (Table 3). The overestimation also happens for altostratus over cumulus and strati-form clouds. However, the overlap of high cloud with altocumulus and cumulus are underestimated by -32.6% and -25% over land during daytime, respectively. The underestimations (or overestimations) of cloud fraction by random overlap assumption finally can cause the overestimations (or underestimations) of cloud radiative effects. For example, the overestimations of cloud radiative effect are obvious for High+St/Sc and Ac+St/Sc (about 3.9 W/m^2 at surface) and As+St/Sc (about 3.9 W/m^2 at surface), whereas the underestimations of cloud radiative effect are obvious for High+Ac and High+Cu (Table 3). For nighttime, the differences of overlap fraction are similar (Table 4). In summary, the difference between $C_{overlap}$ and C_{real} are more obvious for high cloud over altocumulus, strati-form clouds and altocumulus over strati-form clouds.

5. Summary and discussion

Although cloud types and their co-occurrence variations are the most significant components of the global climate system and cloud climatology studies, systematic researches about their statistical properties on a global extent still have received much less attention. This study quantitatively evaluates the co-occurrence frequencies of different cloud types, analyzes their along-track horizontal scales and radiative effects by using the latest cloud classification (2B-CLDCLASS-Lidar) and radiative fluxes products (2B-FLXHR-LIDAR) based on the 4 years' combined measurements of CALIPSO and CloudSat. In addition, we also preliminary evaluate the cloud overlap assumptions and compare the global average cloud fraction of each cloud type by using four different datasets. Although some statistical results are in reasonable agreement with previous works, additional new insights are gained in this paper.

The statistical results clearly show the high cloud, altostratus, altocumulus and cumulus types are much more likely to co-exist with other cloud types. However, the stratus/stratocumulus and nimbostratus, which typically are under large-scale subsidence regions, and convective clouds are much more likely to exhibit individual feature. General speaking, the High-over-St/Sc and High-over-Cu cloud systems are more popular over the vast ocean of the tropics and mid-latitudes, while High-over-Ac cloud systems tend to prevail over the land in the same latitudes. In addition, the As-over-St/Sc cloud systems are dominant in the high-latitudes. The zonal variations of along-track horizontal scale also are obvious distinct for different multilayered cloud systems. For global averages, As+St/Sc has maximum scale (17.4 km) and STD (23.5 km), while Ac+Cu has minimum scale (2.8 km) and STD (3.1 km). Generally speaking, the percentages of radiative contribution from multilayered cloud systems reach 40.1% (about -41.3 W/m^2) and 42.3% ((about -50.2 W/m^2) at TOA and surface, respectively. However, the radiative effects of ten multilayered cloud types which we study reach -22.7 W/m^2 and -27.1 W/m^2 at TOA and surface (contribution: 22%) during daytime, respectively. High+Ac and High+Sc/St (or Cu) cloud systems are predominant in the weighted global mean cloud radiative effects due to their more frequent occurrence.

The active sensors allow us to preliminary evaluate how well the overlap assumptions can describe the real overlap of two separated cloud types. The results show that differences still exist even if the random cloud overlap assumption is thought to better describe cloud overlap behavior than other schemes for two separated cloud layers or types. In summary, the cloud fractions based on the random overlap assumption mainly leads to an underestimation over the vast ocean except for the west-central Pacific Ocean warm pool. Obvious overestimations are primarily occurring in the lands areas of the tropics and subtropics, particularly in regions with low multilayered cloud fractions. In view of negative overlap parameters main occur over the vast ocean, especially over the ocean of 40°S pole-ward, thus we suggest that a linear combination of minimum and random overlap assumptions possible may further improve the predictions of real cloud fraction for those multilayered cloud types (e.g. As+St/Sc and Ac+St/Sc) over Southern oceans, which possible are partially responsible for TOA shortwave radiation bias in the climate models over this region (Haynes et al., 2011). However, the positive overlap parameters almost locate the lands of tropics and subtropics and the Antarctic continent, it indicates that random overlap or exponential random overlap still can works well at these areas.

Although many previous studies already quantitatively evaluates the global mean cloud fraction of each cloud type by using different datasets, some difference in the results from several datasets still are inevitable and obvious because of different approaches and limitations (see Table 5). Generally speaking, compared to the results from Radar-only cloud classification, the new results from Radar-Lidar cloud classification are in more reasonable agreement with at least one of the other datasets, typically ISCCP. However, we also find some new features, which weren't observed by using the ISCCP D1 dataset (Doutriaux-Boucher and Seze, 1998). For example, altostratus and altocumulus prevail over the arid/semi-arid land of the Northern Hemisphere (northwestern part of China and North America) and the Southern Hemisphere (Australia and the southern part of Africa), respectively. Although the representations and simulations of these middle-level clouds in global climate models still are poor and under-predicted (Zhang et al., 2005), it is certain that the balance of phases for these mixed-phase clouds (that is, midlevel clouds) due to any cloud layer temperature or ice nuclei (IN) change will cause a potentially large radiative impact in local regions (Sassen and Khvorostyanov, 2007). Thus, in order to better quantify the feedback of an individual cloud type to these regions and document the local cloud climatology, related studies with midlevel clouds over these arid/semi-arid regions should probably be focused on the impact of dust aerosol on their radiative effects and so-called "cold rain process" (Huang et al., 2006c; 2006d; Su et al., 2008; Wang et al., 2010).

Acknowledgments. This research was supported jointly supported by the National Basic Research Program of China under No. 2013CB955802, No. 2012CB955301, the National Science Foundation of China under grant 41205015, the Developmental Program of Changjiang Scholarship and Innovative Research Team (IRT1018), and China 111 project (No. B13045). We also would like to thank the CALIPSO, and CloudSat science teams for providing excellent and accessible data products that made this study possible.

References

Ackerman, T. P., Liou, K.N., Valero, F. P. J., and Pfister, L.: Heating rates in tropical anvils, J. Atmos. Sci., 45, 1606–1623, 1988.

Barker, H.W.: Overlap of fractional cloud for radiation calculations in GCMs: a global analysis using CloudSat and CALIPSO data, J. Geophys. Res., 113, D00A01, doi:10.1029/2007JD009677, 2008.

Baum, B. A. and Wielicki, B. A.: Cirrus Cloud Retrieval Using Infrared Sounding Data: Multilevel Cloud Errors, J. Appl. Meteor., 33, 107–117, 1994.

Behrangi, A., Kubar, T., and Lambrigtsen, B. H.: Phenomenological Description of Tropical Clouds Using CloudSat Cloud Classification, Mon. Weather. Rev., 140, 3235–3249, 2012.

Betts, A. K. and Boers, R.: A cloudiness transition in a marine boundary layer, J. Atmos. Sci., 47, 1480–1497, 1990.

Cess, R. D., Potter, G. L., Blanchet, J. P., Boer, G. J., Del Genio, A. D., Déqué, M., Dymnikov, V., Galin, V., Gates, W. L., Ghan, S. J., Kiehl, J. T., Lacis, A. A., Le Treut, H., Li, Z. X., Liang, X.Z., McAvaney, B. J., Meleshko, V. P., Mitchell, J. F. B., Morcrette, J. J., Randall, D. A., Rikus, L., Roeckner, E., Royer, J. F., Schlese, U., Sheinin, D. A., Slingo, A., Sokolov, A. P., Taylor, K.E., Washington, W. M., Wetherald, R. T., Yagai, I., and Zhang, M. H.: Intercomparison and interpretation of climate feedback processes in 19 atmospheric general circulation models, J. Geophys. Res., 95, 16601–16615, 1990.

Chang, F. L. and Li, Z.: A new method for detection of cirrus overlapping- low clouds and determination of their optical properties, J. Atmos. Sci., 62, 3993–4009, 2005a.

Chang, F. L. and Li, Z.: A near global climatology of single-layer and overlapped clouds and their optical properties retrieved from TERRA/MODIS data using a new algorithm, J. Clim., 18, 4752–4771, 2005b.

Chen, B., Huang, J., Minnis, P., Hu, Y., Yi, Y., Liu, Z., Zhang, D., and Wang, X.: Detection of dust aerosol by combining CALIPSO active lidar and passive IIR measurements, Atmos. Chem. Phys., 10, 4241-4251, 2010.

Chen, C. and Cotton, W. R.: The physics of the marine stratocumulus- capped mixed layer, J. Atmos. Sci., 44, 2951–2977, 1987.

Chen, T., Rossow, W. B., and Zhang, Y.: Radiative Effects of Cloud-Type Variations, J. Clim., 13, 264–286, 2000.

Choi, Y.S., Lindzen, R.S., Ho, C.H., and Kim, J.: Space observations of cold-cloud phase change, Proc. Natl Acad. Sci., 107, 11211–11216, 2010.

Doutriaux-Boucher, M. and Seze, G.: Significant changes between the ISCCP C and D cloud climatologies, Geophys. Res. Lett., 25, 4193-4196, 1998.

Eastman, R. and Warren, S. G.: A 39-Yr Survey of Cloud Changes from Land Stations Worldwide 1971–2009: Long-Term Trends, Relation to Aerosols, and Expansion of the Tropical Belt, J. Clim., 26, 1286-1303, 2013.

Eastman, R., Warren, S. G., and Hahn, C. J.: Variations in Cloud Cover and Cloud Types over the Ocean from Surface Observations, 1954–2008, J. Clim., 24, 5914–5934, doi: 10.1175/2011JCLI3972.1, 2011.

Hagihara, Y., Okamoto, H., and Yoshida, R.: Development of a combined CloudSat/CALIPSO cloud mask to show global cloud distribution, J. Geophys. Res., 115, D00H33, doi:10.1029/2009JD012344, 2010.

Hahn, C. J. and Warren, S. G.: Extended edited cloud reports from ships and land stations over the globe, 1952– 1996, Numer. Data Package NDP-026C, 79 pp., Carbon Dioxide Inf. Anal. Cent., Dep. of Energy, Oak Ridge, Tenn, 1999.

Hahn, C. J., Rossow, W. B., and Warren, S. G.: ISCCP Cloud Properties Associated with Standard Cloud Types Identified in Individual Surface Observations, J. Clim., 14, 11–28, 2001.

Han, Q., Rossow, W. B., and Lacis, A. A.: Near-global survey of effective droplet radii in liquid water clouds using ISCCP data, J. Clim., 7, 465-497, 1994.

Hartmann, D. L., Ockert-Bell, M. E., and Michelsen, M.L.: The effect of cloud type on Earth’s energy balance: global analysis, J. Clim., 5, 1281–1304, 1992.

Haynes, J.M., Jakob, C., Rossow, W.B., Tselioudis, G., and Brown, J.: Major Characteristics of Southern Ocean Cloud Regimes and Their Effects on the Energy Budget, J. Clim., 24, 5061-5080. doi: 10.1175/2011JCLI4052.1, 2011.

Haynes, J.M., Vonder-Haar, T.H., L’Ecuyer, T., Henderson, D.: Radiative heating characteristics of Earth’s cloudy atmosphere from vertically resolved active sensors, Geophys. Res. Lett., 40, 624–630, doi:10.1002/grl.50145, 2013.

Henderson, D.S., L’Ecuyer, T., Stephens, G., Partain, P., and Sekiguchi, M.: A multi-sensor perspective on the radiative impacts of clouds and aerosols, J. Appl. Meteorol. Climatol., 52, 853–871, doi: 10.1175/JAMC-D-12-025.1, 2013.

Hogan, R. J. and Illingworth, A. J.: Deriving cloud overlap statistics from radar, Q. J. Roy. Meteor. Soc., 128, 2903–2909, 2000.

Huang, J.P.: Analysis of ice water path retrieval errors over tropical ocean, Advances in Atmospheric Sciences, 23: 165-180, 2006a.

Huang, J. P., Minnis, P., and Lin, B.: Advanced retrievals of multilayered cloud properties using multispectral measurements, J. Geophys. Res., 110, D15S18, doi:10.1029/2004JD005101, 2005.

Huang, J. P., Minnis, P., and Lin, B.: Determination of ice water path in ice-over-water cloud systems using combined MODIS and AMSR-E measurements, Geophys. Res. Lett., 33, L21801, doi:10.1029/ 2006GL027038, 2006b.

Huang, J.P., Lin, B., Minnis, P., Wang, T., Wang, X., Hu, Y., Yi, Y., and Ayers, J.R.: Satellite-based assessment of possible dust aerosols semi-direct effect on cloud water path over East Asia, Geophys. Res. Lett., 33, L19802, doi: 10.1029/2006GL026561, 2006c.

Huang, J.P., Minnis, P., Lin, B., Wang, T., Yi, Y., Hu, Y., Sun-Mack, S., and Ayers, K.: Possible influences of Asian dust aerosols on cloud properties and radiative forcing observed from MODIS and CERES, Geophys. Res. Lett., 33, L06824, doi: 10.1029/2005GL024724, 2006d.

Kato, S., Sun-Mack, S., Miller, W. F., Rose, F. G., Chen, Y., Minnis, P., and Wielicki, B. A.: Relationships among cloud occurrence frequency, overlap, and effective thickness derived from CALIPSO and CloudSat merged cloud vertical profiles, J. Geophys. Res., 115, D00H28, doi:10.1029/2009JD012277, 2010.

Klein, S. A. and Hartmann, D. L.: The seasonal cycle of low stratiform clouds, J. Clim., 6, 1588–1606, 1993.

L’Ecuyer, T.S., Wood, N., Haladay, T., and Stephens, G.L.: The impact of clouds on atmospheric heating based on the R04 CloudSat fluxes and heating rate dataset, J. Geophys. Res., 113, D00A15, doi:10.1029/2008JD009951, 2008.

Li, J., Yi, Y., Minnis, P., Huang, J., Yan, H., Ma, Y., Wang, W., and Ayers, k.:

Radiative effect differences between multi-layered and single-layer clouds derived from CERES, CALIPSO, and CloudSat data, J. Quant. Spectrosc. Radiat. Transf., 112, 361–375, 2011.
Liang, X.Z., and Wu, X.: Evaluation of a GCM subgrid cloudradiation interaction parameterization using cloud-resolving model simulations, Geophys. Res. Lett., 32, L06801, doi:10.1029/2004 GL022301, 2005.
Liao, X., Rossow, W. B., and Rind, D.: Comparison between SAGE II and ISCCP high-level clouds. Part I: Global and zonal mean cloud amounts, J. Geophys. Res., 100, 1121–1135, 1995.
Luo, Y., Zhang, R., and Wang, H.: Comparing occurrences and vertical structures of hydrometeors between the eastern China and the Indian monsoon region using CloudSat/CALIPSO data, J. Clim., 22, 1052-1064, 2009.
Minnis, P., Yi, Y., Huang, J., and Ayers, J. K.: Relationships between radiosonde and RUC-2 meteorological conditions and cloud occurrence determined from ARM data, J. Geophys. Res., 110, D23204, doi:10.1029/2005JD006005, 2005.
Minnis, P., Huang, J., Lin, B., Yi, Y., Arduim, R., Fan, T.-F., Ayers, J. K., and Mace, G. G.: Ice cloud properties in ice-over-water cloud systems using Tropical Rainfall Measuring Mission (TRMM) visible and infrared scanner and TRMM Microwave Imager data, J. Geophys. Res., 112, D06206, doi: 10.1029/2006JD007626, 2007.
Moran, J.M., Morgan, M.D., and Pauley, P.M.: *Meteorology: The Atmosphere and the Science of Weather*, Prentice Hall, New Jersey, 530pp, 1997.
Morcrette, J. J. and Jakob, C.: The response of the ECMWF model to changes in the cloud overlap assumption, Mon. Weather. Rev., 128, 1707–1732, 2000.
Norris, J. R. and Leovy, C. B.: Interannual variability in stratiform cloudiness and sea surface temperature, J. Clim., 7, 1915–1925, 1994.
Parker, S.P.: *Meteorology Source Book*. McGraw-Hill, New York, 304 pp, 1988.
Rossow, W. B. and Schiffer, R. A.: ISCCP cloud data products, B. Am. Meteorol. Soc., 72, 2–20, 1991.
Rossow, W. B. and Schiffer, R. A.: Advances in understanding clouds from ISCCP, B.

Am. Meteorol. Soc., 80, 2261– 2286, 1999.

Sassen, K. and Cho, B. S.: Subvisual–thin cirrus lidar dataset for satellite verification and climatological research, J. Appl. Meteor., 31, 1275–1285, 1992.

Sassen, K., and Khvorostyanov, V.I.: Microphysical and radiative properties of mixed phase altocumulus: a model evaluation of glaciation effects. Atmos. Res., 84, 390–398, 2007.

Sassen, K. and Wang, Z.: Classifying clouds around the globe with the CloudSat radar: 1-year of results, Geophys. Res. Lett., 35, L04805, doi:10.1029/2007GL032591, 2008.

Sassen, K., Wang, Z., and Liu, D.: Cirrus clouds and deep convection in the tropics: Insights from CALIPSO and CloudSat, J. Geophys. Res., 114, D00H06, doi:10.1029/2009JD011916, 2009.

Stephens, G. L.: Cloud feedbacks in the climate system: a critical review, J. Clim., 18, 237–273, 2005.

Stephens, G. L., Wood, N. B., and Gabriel, P. M.: An assessment of the parameterization of subgrid-scale cloud effects on radiative transfer: Part I. Vertical overlap, J. Atmos. Sci., 61, 715–732, 2004.

Stephens, G.L., Vane, D.G., Boain, R.J., Mace, G.G., Sassen, K., Wang, Z., Illingworth, A.J., O'Connor, E.J., Rossow, W.B., Durden, S.L., Miller, S.D., Austin, R.T., Benedetti, A., Mitrescu, C., and CloudSat Science Team.: The CloudSat mission and the A-Train, A new dimension of space-based observations of clouds and precipitation, B. Am. Meteorol. Soc., 83, 1771–1790, 2002.

Su, J., Huang, J., Fu, Q., Minnis, P., Ge, J., and Bi, J.: Estimation of Asian dust aerosol effect on cloud radiation forcing using Fu-Liou radiative model and CERES measurements, Atmos. Chem. Phys., 8, 2763-2771, 2008.

Tian, L. and Curry, J. A.: Cloud overlap statistics, J. Geophys. Res., 94, 9925−9935, 1989.

Trenberth, K.E., and Fasullo, J.T.: Simulation of present-day and twenty-first-century energy budgets of the southern oceans, J. Clim., 23, 440–454, 2010.

Wang, L. and Dessler, A. E.: Instantaneous cloud overlap statistics in the tropical area revealed by ICESat/GLAS data, Geophys. Res. Lett., 33, L15804, doi:10.1029/2005GL024350, 2006.

Wang, Z. and Sassen, K.: Cloud type and macrophysical property retrieval using multiple remote sensors, J. Appl. Meteor., 40, 1665–1682, 2001.

Wang, W., Huang, J., Minnis, P., Hu, Y., Li, J., Huang, Z., Ayers, J. K., and Wang, T.: Dusty cloud properties and radiative forcing over dust source and downwind regions derived from A-Train data during the Pacific Dust Experiment, J. Geophys. Res., 115, D00H35, doi: 10.1029/2010JD014109, 2010.

Warren, S. G., Eastman, R. M., and Hahn, C. J.: A survey of changes in cloud cover and cloud types over land from surface observations, 1971–96, J. Clim., 20, 717–738, 2007.

Warren, S. G., Hahn, C. J., and London, J.: Simultaneous occurrence of different cloud types, J. Clim. Appl. Meteorol., 24, 658–67, 1985.

Winker D. M., Hunt, W. H., and Mcgill, M. J.: Initial performance assessment of CALIOP, Geophys. Res. Lett., 34, L19803, doi:10.1029/ 2007GL030135, 2007.

World Meteorological Organization.: *International Cloud Atlas: Abridged atlas*, World Meteorological Organization, 62 pp., and 72 plates, Geneva, 1956.

Wylie, D.P., Eloranta, E., Spinhirne, J.D., and Palm, S.P.: A comparison of cloud cover statistics from the GLAS lidar with HIRS, J. Clim., 20, 4968–4981, doi:10.1175/JCLI4269.1, 2007.

Yu, R. C., Wang, B., and Zhou, T.: Climate effects of the deep continental stratus clouds generated by the Tibetan Plateau, J. Clim., 17, 2702-2713, 2004.

Yu, H., Remer, L. A., Chin, M., Bian, H., Tan, Q., Yuan, T., and Zhang, Y.: Aerosols from overseas rival domestic emissions over North America, Science, 337(6094), 566–569, doi:10.1126/science.1217576, 2012.

Yuan, T. and Oreopoulos, L.: On the global character of overlap between low and high clouds, Geophys. Res. Lett., 40, 5320–5326, doi:10.1002/grl.50871, 2013.

Zhang, D., Luo, T., Liu, D., and Wang, Z.: Spatial Scales of Altocumulus Clouds Observed with Collocated CALIPSO and CloudSat Measurements, Atmos. Res., 148, 58-69, doi: 10.1016/j.atmosres.2014.05.023, 2014.

Zhang, M. H., Lin, W. Y., Klein, S. A., Bacmeister, J. T., Bony, S., Cederwall, R. T., Del Genio, A.D., Hack, J. J., Loeb, N. G., Lohmann, U., Minnis, P., Musat, I., Pincus, R., Stier, P., Suarez,M. J., Webb, M. J., Wu, J. B., Xie, S. C., Yao, M. S., and Zhang, J. H.: Comparing clouds and 15 their seasonal variations in 10 atmospheric general circulation models with satellite measurements, J. Geophys. Res., 110, D15S02, doi:10.1029/2004JD005021, 2005.

Table 1. Globally averaged overlapping percentages of different cloud types over land and ocean during daytime.

	SL[a]	ML[b]	High	As	Ac	St/Sc	Cu	Ns	Deep	surface
High	8.8	14.5	3.7	2.5	4.3	3.2	2.8	1.0	0.4	Land
	8.8	**16.4**	**4.1**	**2.2**	**3.5**	**5.2**	**3.5**	**1.2**	**0.3**	**Ocean**
As	6.5	6.7	--	0.9	1.0	2.0	1.1	0.4	--	Land
	4.2	**6.1**	**--**	**0.5**	**0.9**	**2.5**	**1.0**	**0.3**	**--**	**Ocean**
Ac	5.3	7.0	--	0.01	1.1	0.9	1.1	0.04	--	Land
	3.1	**6.4**	**--**	**0.01**	**0.8**	**1.5**	**1.0**	**0.08**	**--**	**Ocean**
St/Sc	10.5	6.2	--	--	--	0.3	0.5	--	--	Land
	21.9	**9.4**	**--**	**--**	**--**	**0.4**	**0.7**	**--**	**--**	**Ocean**
Cu	3.9	5.1	--	--	--	0.1	0.3	--	--	Land
	6.6	**5.9**	**--**	**--**	**--**	**0.2**	**0.3**	**--**	**--**	**Ocean**
Ns	4.0	1.5	--	--	--	0.02	0.09	--	--	Land
	4.1	**1.6**	**--**	**--**	**--**	**0.02**	**0.05**	**--**	**--**	**Ocean**
Deep	0.8	0.4	--	--	--	--	--	--	--	Land
	0.8	**0.3**	**--**	**--**	**--**	**--**	**--**	**--**	**--**	**Ocean**

[a]The SL represents the single-layered cloud. [b]The ML represents the multi-layered cloud. And, those boldfaced values indicated the overlapping percentages of different cloud types over ocean.

Table 2. Globally averaged overlapping percentages for different cloud types over land and ocean during nighttime.

	SL[a]	ML[b]	High	As	Ac	St/Sc	Cu	Ns	Deep	surface
High	12.0	17.4	5.5	3.2	6.6	2.6	1.8	1.3	0.3	Land
	8.8	**20.8**	**4.7**	**2.3**	**5.0**	**7.6**	**4.4**	**1.3**	**0.3**	**Ocean**
As	6.9	7.4	--	1.0	1.1	1.9	0.9	0.4	--	Land
	3.9	**6.3**	**--**	**0.4**	**0.9**	**2.6**	**1.0**	**0.3**	**--**	**Ocean**
Ac	4.6	8.5	--	0.01	1.2	0.7	0.6	0.05	--	Land
	3.1	**8.1**	**--**	**0.01**	**1.0**	**1.9**	**1.2**	**0.08**	**--**	**Ocean**
St/Sc	6.4	5.1	--	--	--	0.2	0.3	--	--	Land
	23.8	**12.1**	**--**	**--**	**--**	**0.4**	**0.8**	**--**	**--**	**Ocean**
Cu	2.0	3.4	--	--	--	0.1	0.2	--	--	Land
	5.9	**6.9**	**--**	**--**	**--**	**0.2**	**0.4**	**--**	**--**	**Ocean**
Ns	3.9	1.7	--	--	--	--	0.08	--	--	Land
	4.0	**1.7**	**--**	**--**	**--**	**--**	**0.05**	**--**	**--**	**Ocean**
Deep	0.8	0.3	--	--	--	--	--	--	--	Land
	0.9	**0.3**	**--**	**--**	**--**	**--**	**--**	**--**	**--**	**Ocean**

[a]The SL represents the single-layered cloud. [b]The ML represents the multi-layered cloud. And, those boldfaced values indicated the overlapping percentages of different cloud types over ocean.

Table 3. Cloud fractions of different multilayered cloud types based on different overlap assumptions and observations during daytime. Here, $C_{overlap}$ and $C_1 \times C_2$ are the overlap cloud fraction from observations and overlap assumptions. "*a*" presents the overlap parameter.

Cloud type	C_{max}	C_{random}	C_{real}	$C_1 \times C_2$	$C_{overlap}$	R[a] (W/m^2)	Diff.[b]	*a*
High+As	23.3	33.4	34.0	3.1	2.5	0.8	24.0%	-0.06
	(25.2)	**(32.9)**	**(33.3)**	**(2.6)**	**(2.2)**	**(0.8)**	**(18.2%)**	**(-0.05)**
High+Ac	23.3	32.7	31.3	2.9	4.3	-2.4	-32.6%	0.15
	(25.2)	**(32.3)**	**(31.2)**	**(2.4)**	**(3.5)**	**(-2.3)**	**(-31.4%)**	**(0.15)**
High+St/Sc	23.3	36.1	36.8	3.9	3.2	1.0	21.9%	-0.05
	(31.3)	**(48.6)**	**(51.3)**	**(7.9)**	**(5.2)**	**(3.9)**	**(51.9%)**	**(-0.16)**
High+Cu	23.3	30.2	29.5	2.1	2.8	-1.3	-25.0%	0.1
	(25.2)	**(34.5)**	**(34.2)**	**(3.2)**	**(3.5)**	**(-0.7)**	**(-8.6%)**	**(0.03)**
High+Ns	23.3	27.5	27.8	1.3	1.0	0.7	30.0%	-0.07
	(25.2)	**(29.5)**	**(29.7)**	**(1.4)**	**(1.2)**	**(0.5)**	**(16.7%)**	**(-0.05)**
High+Deep	23.3	24.2	24.1	0.3	0.4	-0.1	-25.0%	0.11
	(25.2)	**(26.0)**	**(26.0)**	**(0.3)**	**(0.3)**	**(0.0)**	**(0.0%)**	**(0.0)**
As+St/Sc	16.7	27.7	27.9	2.2	2.0	0.6	10.0%	-0.02
	(31.3)	**(38.4)**	**(39.1)**	**(3.2)**	**(2.5)**	**(2.5)**	**(28.0%)**	**(-0.1)**
As+Cu	13.2	21.0	21.1	1.2	1.1	0.4	9.1%	-0.01
	(12.5)	**(21.5)**	**(21.8)**	**(1.3)**	**(1.0)**	**(1.7)**	**(30.0%)**	**(-0.03)**
Ac+St/Sc	16.7	26.9	28.1	2.1	0.9	2.2	133.3%	-0.12
	(31.3)	**(37.8)**	**(39.3)**	**(3.0)**	**(1.5)**	**(3.9)**	**(100.0%)**	**(-0.23)**
Ac+Cu	12.3	20.2	20.2	1.1	1.1	0.0	0.0%	0.0
	(12.5)	**(20.8)**	**(21.0)**	**(1.2)**	**(1.0)**	**(0.5)**	**(20.0%)**	**(-0.02)**

[a]Calculated from (C_{random}-C_{real})×(global mean cloud radiative effect of each cloud type). [b]Calculated from ($C_1 \times C_2$-$C_{overlap}$)/ $C_{overlap}$. And, those boldfaced values in the brackets indicated the overlapping percentages of different cloud types over ocean surface. But for R[a], the values indicated the cloud radiative effect difference between real and random overlap at TOA and Surface (in the brackets), respectively. Here, only cloud radiative effects during daytime are considered.

Table 4. Cloud fractions of different multilayered cloud types based on different overlap assumptions and observations during nighttime. Here, $C_{overlap}$ and $C_1 \times C_2$ are the overlap cloud fraction from observations and overlap assumptions. "*a*" presents the overlap parameter.

Cloud type	C_{max}	C_{random}	C_{real}	$C_1 \times C_2$	$C_{overlap}$	R[a](W/m^2)	Diff.[b]	*a*
High+As	29.4	39.5	40.5	4.2	3.2	-	31.3%	-0.1
	(29.6)	**(36.8)**	**(37.5)**	**(3.0)**	**(2.3)**	-	**(30.4%)**	**(-0.1)**
High+Ac	29.4	38.6	35.9	3.9	6.6	-	-40.9%	0.29
	(29.6)	**(37.5)**	**(35.8)**	**(3.3)**	**(5.0)**	-	**(-34.0%)**	**(0.22)**
High+St/Sc	29.4	37.5	38.3	3.4	2.6	-	30.8%	-0.1
	(35.9)	**(54.9)**	**(57.9)**	**(10.6)**	**(7.6)**	-	**(39.5%)**	**(-0.16)**
High+Cu	29.4	33.2	33.0	1.6	1.8	-	-11.1%	0.05
	(29.6)	**(38.6)**	**(38.0)**	**(3.8)**	**(4.4)**	-	**(-13.6%)**	**(0.07)**
High+Ns	29.4	33.4	33.7	1.6	1.3	-	23.1%	-0.08
	(29.6)	**(33.6)**	**(34.0)**	**(1.7)**	**(1.3)**	-	**(30.8%)**	**(-0.1)**
High+Deep	29.4	30.2	30.2	0.3	0.3	-	0.0%	0.0
	(29.6)	**(30.4)**	**(30.5)**	**(0.4)**	**(0.3)**	-	**(33.3%)**	**(-0.13)**
As+St/Sc	14.3	24.2	23.9	1.6	1.9	-	-15.8%	0.03
	(35.9)	**(42.4)**	**(43.5)**	**(3.7)**	**(2.6)**	-	**(42.3%)**	**(-0.17)**
As+Cu	14.3	18.9	18.8	0.8	0.9	-	-11.1%	0.02
	(12.8)	**(21.7)**	**(22.0)**	**(1.3)**	**(1.0)**	-	**(30.0%)**	**(-0.03)**
Ac+St/Sc	13.1	23.1	23.9	1.5	0.7	-	114.3%	-0.08
	(35.9)	**(43.1)**	**(45.2)**	**(4.0)**	**(1.9)**	-	**(110.5%)**	**(-0.29)**
Ac+Cu	13.1	17.8	17.9	0.7	0.6	-	16.7%	-0.02
	(12.8)	**(22.6)**	**(22.8)**	**(1.4)**	**(1.2)**	-	**(16.7%)**	**(-0.02)**

[a]Calculated from (C_{random}-C_{real})×(global mean cloud radiative effect of each cloud type). [b]Calculated from ($C_1 \times C_2$-$C_{overlap}$)/ $C_{overlap}$. And, those boldfaced values in the brackets indicated the overlapping percentages of different cloud types over ocean surface. But for R[a], the values indicated the cloud radiative effect difference between real and random overlap at TOA and Surface (in the brackets), respectively. Here, only cloud radiative effects during daytime are considered.

Table 5. Comparison of Global cloud type occurrence frequency averages over land and ocean by using four different datasets. CloudSat (Radar-Lidar cloud classification): 2B-CLDCLASS-Lidar product (January/2007-December/2010); CloudSat (Radar-only cloud classification): 2B-CLDCLASS product (June/2006-June/2007). Surface: Annual Means of extended surface observer reports (Hahn and Warren, 1999); ISCCP: ISCCP Annual means from 1986-1993 (Rossow and Schiffer, 1999). Here, the statistical results of the latter three datasets all are from the study of Sassen and Wang (2008).

	CloudSat (Radar-Lidar)[a]		CloudSat (Radar-only)		Surface		ISCCP	
Type	Land	Ocean	Land	Ocean	Land	Ocean	Land	Ocean
High	23.3 (29.4)	25.2 (29.6)	9.6	10.9	23.1	14.0	19.3	15.6
As	13.2 (14.3)	10.3 (10.2)	12.7	12.0	4.8	6.5	8.7	9.7
Ac	12.3 (13.1)	9.5 (11.2)	6.8	6.7	17.2	17.1	8.6	10.2
St+Sc	16.7 (11.5)	31.3 (35.9)	13.5	22.5	18.9	39.4	10.7	18.3
Cu	9.0 (5.4)	12.5 (12.8)	1.7	1.7	4.2	9.8	7.7	12.7
Ns	5.5 (5.6)	5.7 (5.7)	8.6	8.3	6.3	7.9	3.2	3.0
Deep	1.2 (1.1)	1.1 (1.2)	1.8	1.9	3.2	5.3	2.5	2.4

[a] The results from CloudSat (Radar-Lidar) are reported separately for day- and night-time. The values in parentheses indicate the cloud fractions of different cloud types during nighttime.

Figure captions

Figure 1. (a) The global distribution ($2^{\circ}\times2^{\circ}$ grid boxes) of annually averaged multilayered cloud fraction. (b) The zonal distributions of seasonal averaged multilayered cloud fraction.

Figure 2. Zonal distributions of annual most frequently occurring multilayered cloud types based on the 2B-CLDCLASS-Lidar product.

Figure 3. The global distributions of (a) the annual mean dominant cloud types and (b) the corresponding cloud fractions. And, the global distributions of (c) the annual mean dominant multiple cloud types and (d) the corresponding cloud amounts.

Figure 4. (a)-(b):The zonal variation of cloud along-track horizontal scales for these multilayered cloud systems and (c)-(d): their probability distribution.

Figure 5. (a)-(d):The zonal distributions of cloud radiative effect and weighted cloud radiative effect for different multilayered cloud systems at the top of atmosphere (TOA) during daytime.

Figure 6. Same with Figure5, but at the surface during the daytime.

Figure 7. The global average cloud radiative effect and weighted cloud radiative effect for different multilayered cloud types at TOA and surface only during daytime. The gray line presents the global average frequency of occurrence of each cloud type only during daytime (that is, weights). The total weighted cloud radiative effects of whole multilayered cloud system are also showed in the figure 7c and 7d. TOA (-22.7 W/m^2); Surface (-27.1 W/m^2).

Figure 8. (a)-(b): The zonal distributions of the relative difference for different multilayered cloud types and the cumulative relative difference of all multilayered cloud types (gray line). (c)-(d): The zonal distributions of the overlap parameter for different multilayered cloud types and the cumulative overlap parameter of all multilayered cloud types (gray line).

Figure 9. The global distributions of (a) the cumulative relative difference and (b) the cumulative overlap parameter of all multilayered cloud types.

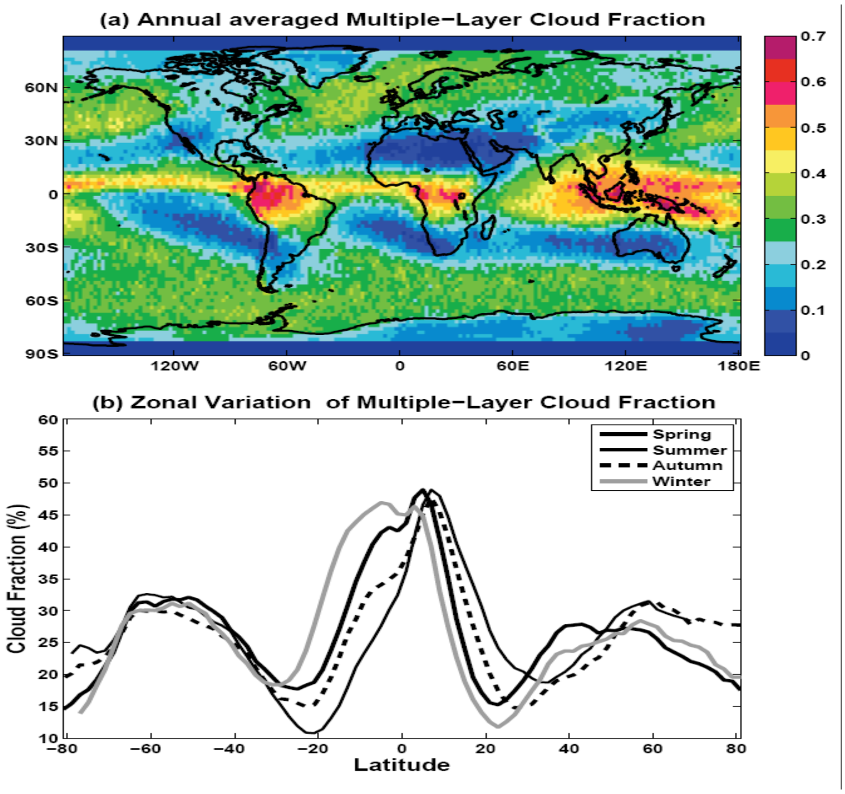

Figure 1. (a) The global distribution (2°×2° grid boxes) of annually averaged multilayered cloud fraction. (b) The zonal distributions of seasonal averaged multilayered cloud fraction.

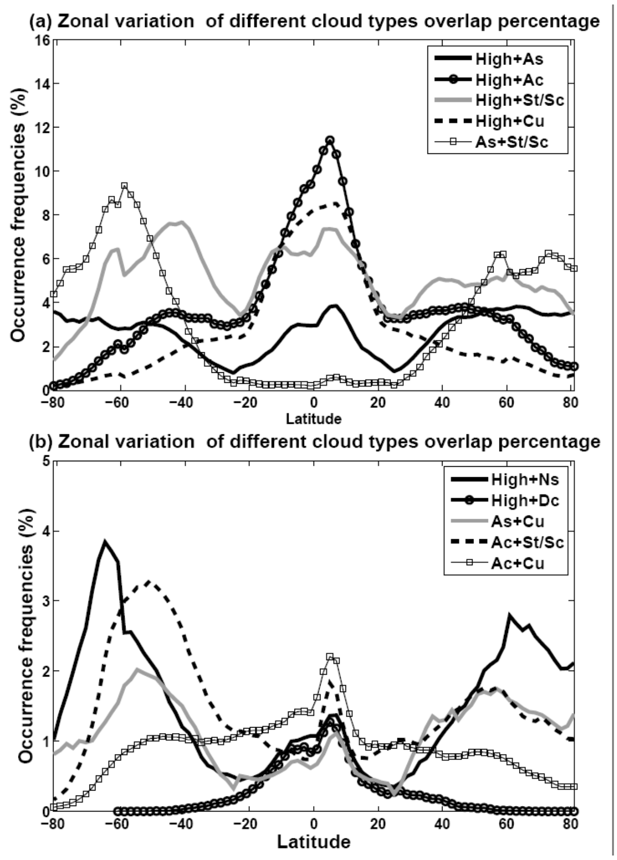

Figure 2. Zonal distributions of annual most frequently occurring multilayered cloud types based on the 2B-CLDCLASS-Lidar product.

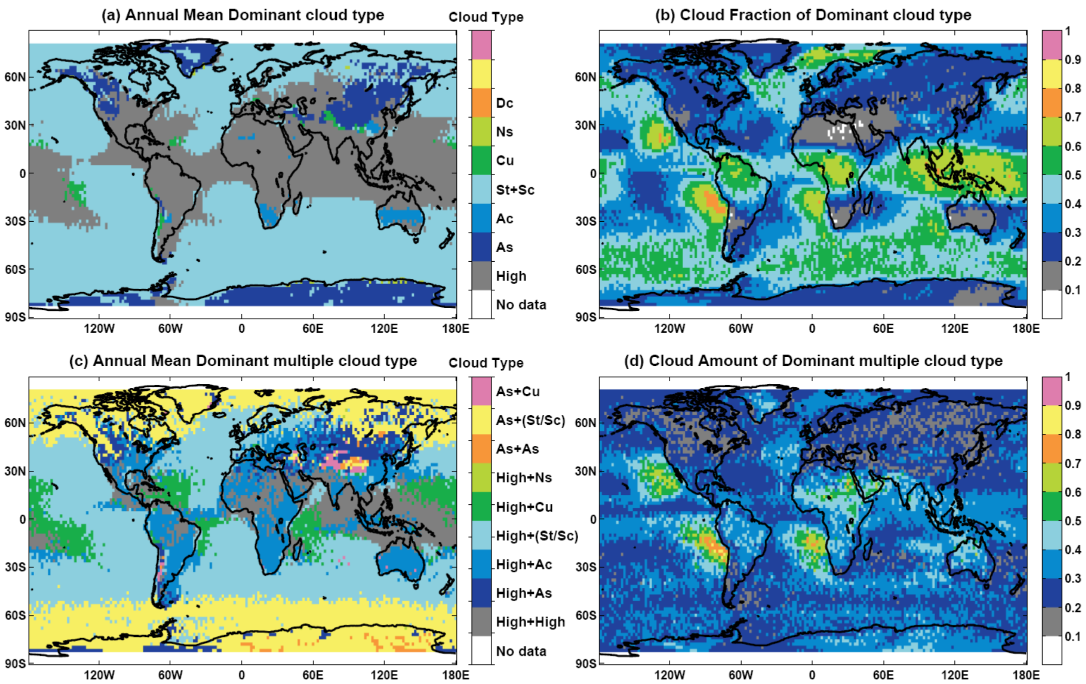

Figure 3. The global distributions of (a) the annual mean dominant cloud types and (b) the corresponding cloud fractions. And, the global distributions of (c) the annual mean dominant multiple cloud types and (d) the corresponding cloud amounts.

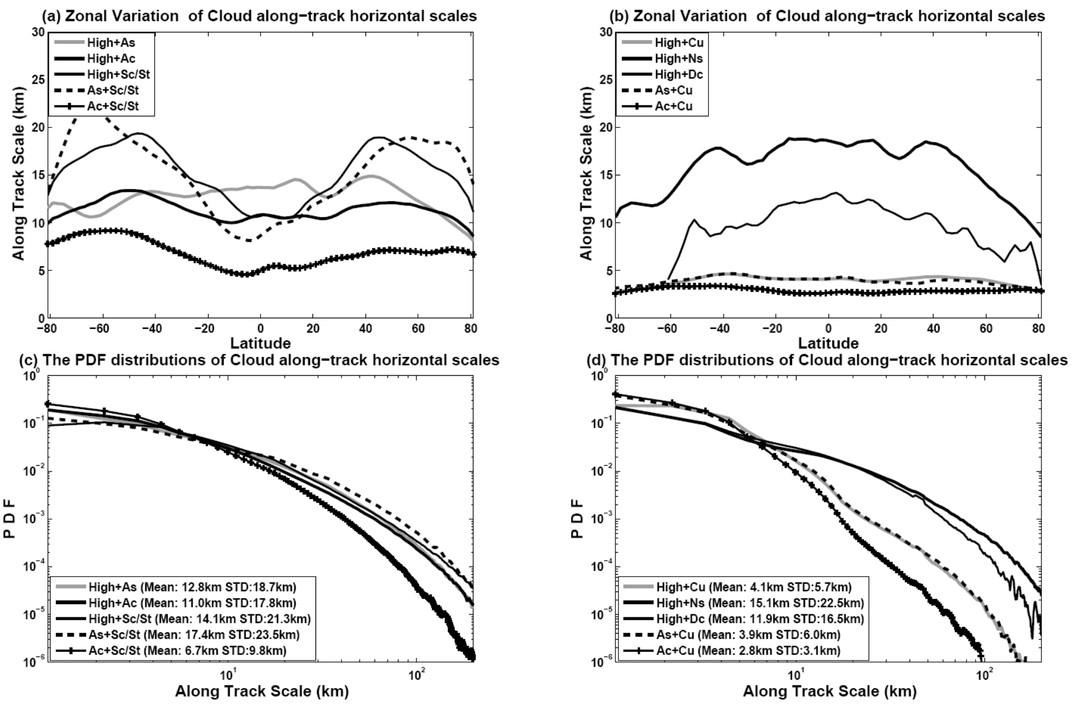

Figure 4. (a)-(b):The zonal variation of cloud along-track horizontal scales for these multilayered cloud systems and (c)-(d): their probability distribution.

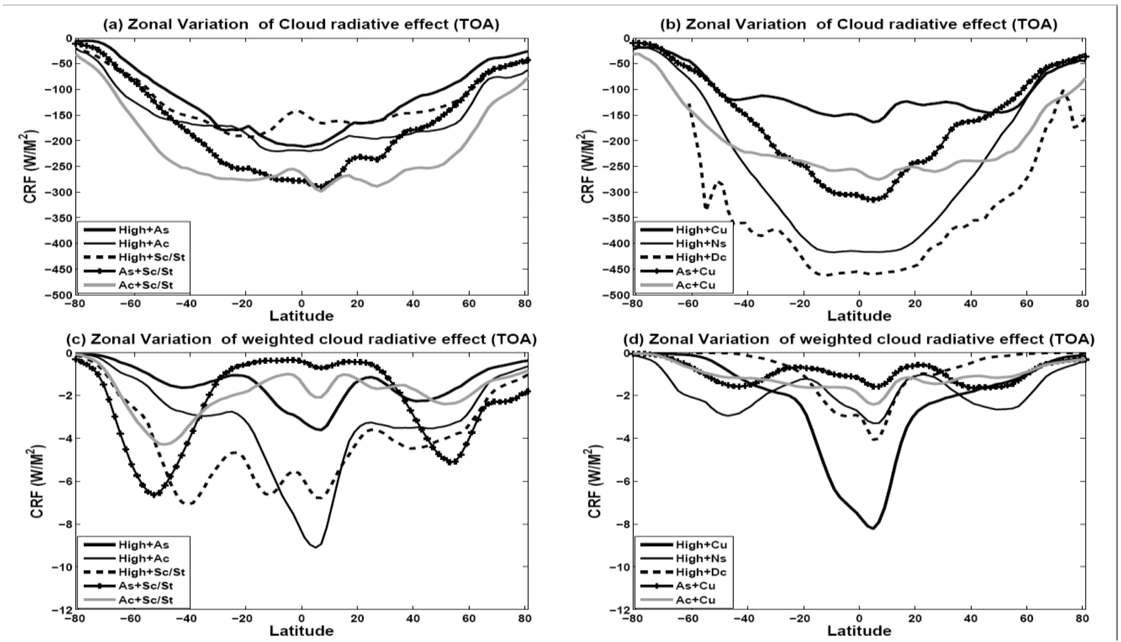

Figure 5. (a)-(d):The zonal distributions of cloud radiative effect and weighted cloud radiative effect for different multilayered cloud systems at the top of atmosphere (TOA) during daytime.

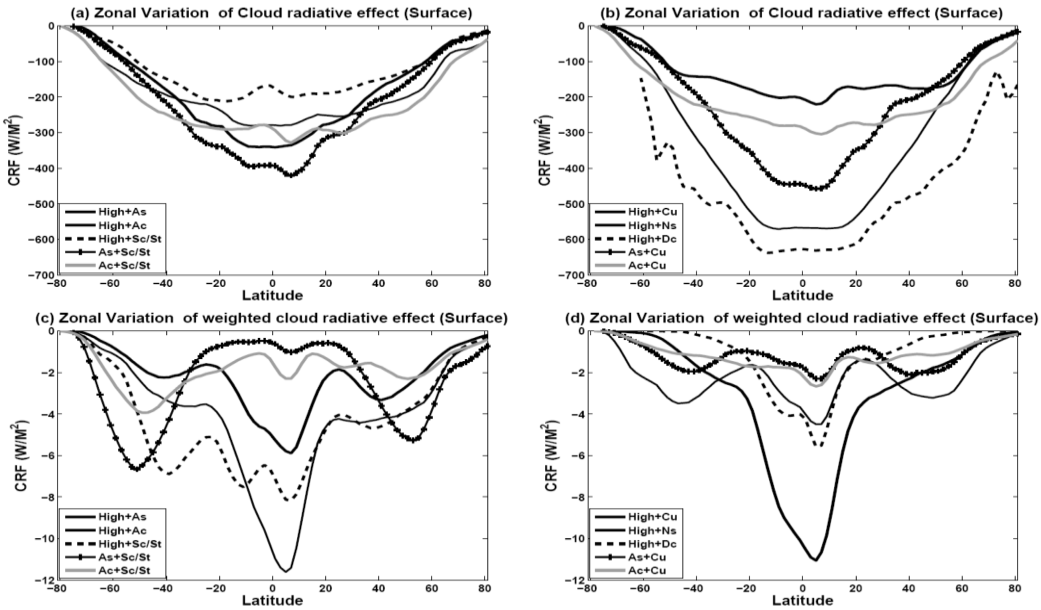

Figure 6. Same with Figure5, but at the surface during the daytime.

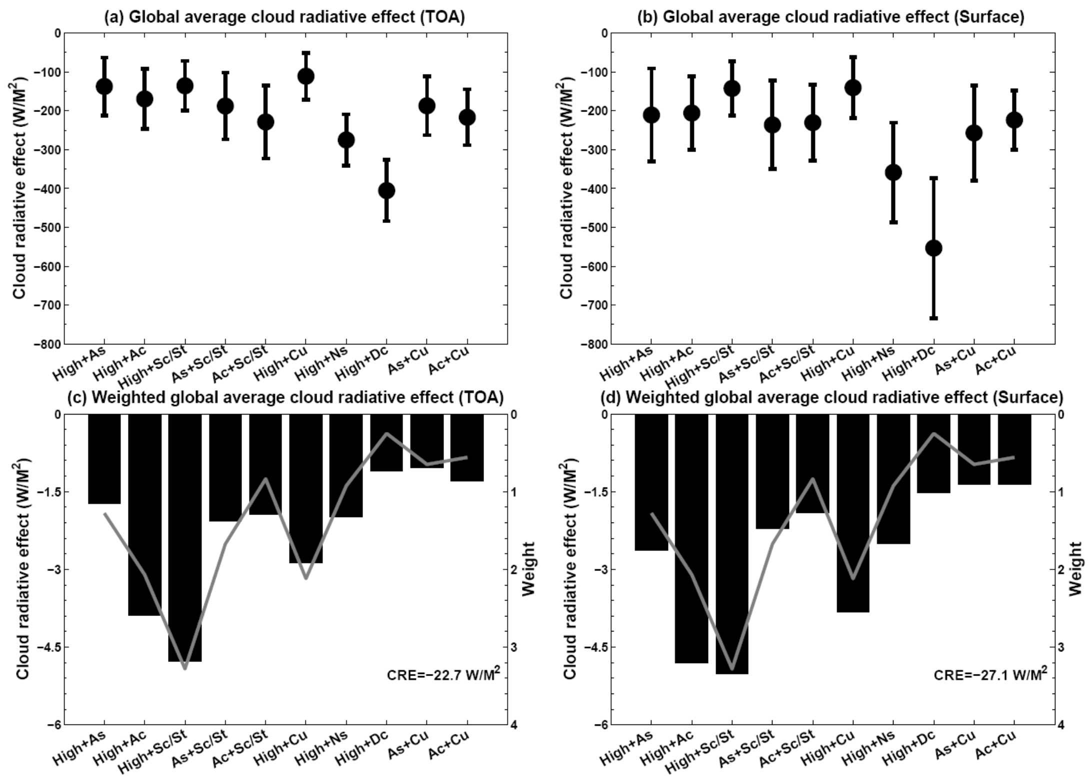

Figure 7. The global average cloud radiative effect and weighted cloud radiative effect for different multilayered cloud types at TOA and surface only during daytime. The gray line presents the global average frequency of occurrence of each cloud type only during daytime (that is, weights). The total weighted cloud radiative effects of whole multilayered cloud system are also showed in the figure 7c and 7d. TOA (-22.7 W/m^2); Surface (-27.1 W/m^2).

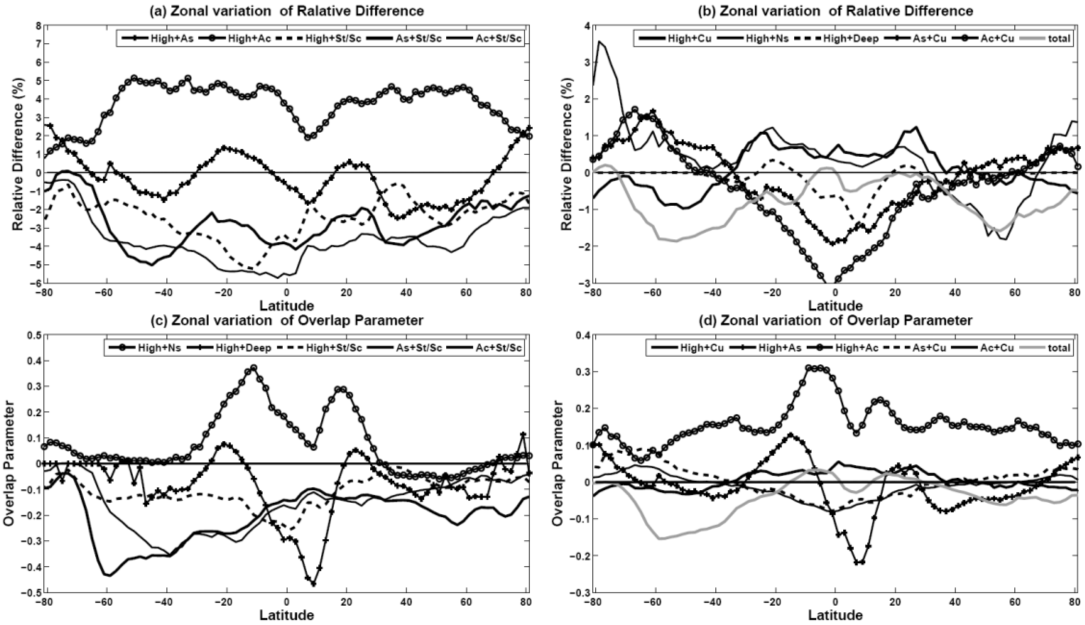

Figure 8. (a)-(b): The zonal distributions of the relative difference for different multilayered cloud types and the cumulative relative difference of all multilayered cloud types (gray line). (c)-(d): The zonal distributions of the overlap parameter for different multilayered cloud types and the cumulative overlap parameter of all multilayered cloud types (gray line).

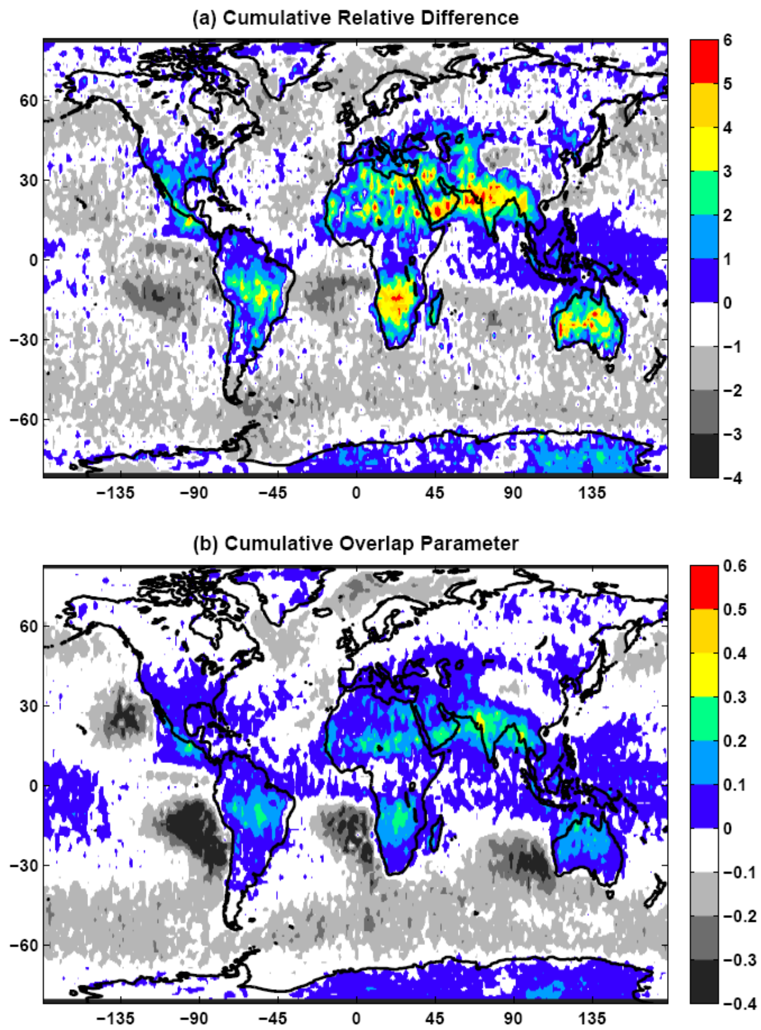

Figure 9. The global distributions of (a) the cumulative relative difference and (b) the cumulative overlap parameter of all multilayered cloud types.